Chinese Chemical Letters 36 (2025) 109815

Contents lists available at ScienceDirect

Chinese Chemical Letters

journal homepage: www.elsevier.com/locate/cclet

In situ imaging of the interfacial processes manipulated by salt concentration on zinc anodes in zinc metal batteries

Jiao Wang[a,b], Shuang-Yan Lang[a,b], Zhen-Zhen Shen[a,b], Gui-Xian Liu[a,b], Jian-Xin Tian[a,b], Yuan Li[a,b], Rui-Zhi Liu[a,b], Rui Wen[a,b,*]

[a] *CAS Key Laboratory of Molecular Nanostructure and Nanotechnology, Beijing National Laboratory for Molecular Sciences, CAS Research/Education Center for Excellence in Molecular Sciences, Institute of Chemistry, Chinese Academy of Sciences, Beijing 100190, China*
[b] *University of Chinese Academy of Sciences, Beijing 100049, China*

ARTICLE INFO

Article history:
Received 2 March 2024
Accepted 22 March 2024
Available online 23 March 2024

Keywords:
In situ AFM
Interfacial processes
Solid electrolyte interphase
Water-in-salt
Zn metal batteries

ABSTRACT

Unstable electrode/electrolyte interfaces and heterogeneous Zn deposition would reduce the Coulombic efficiency and cycle life of Zn metal batteries (ZMBs). Applying water-in-salt (WIS) electrolytes has proven to be an effective strategy to address the above issues. However, an understanding of the reaction mechanisms on the Zn anode at nanoscale is still elusive. Here we utilize *in situ* atomic force microscopy to visualize the solid electrolyte interphase (SEI) formation and Zn deposition/dissolution processes in WIS electrolyte and construct relationships between interfacial behavior and electrochemical performance. The formation processes, chemical properties, and structure of the on-site formed SEI are deeply explored. The SEI with a "plum-pudding" model can guide uniform Zn deposition and reversible dissolution. Mechanistic understanding of the interfacial evolution of the SEI layer and Zn deposition/dissolution has been achieved and will benefit the structural optimization and interfacial engineering of ZMBs.

Given the pressing issues of energy shortage and environmental pollution, there is an urgent need to explore safe, affordable, and sustainable battery systems [1–5]. Zn metal batteries (ZMBs) have gained significant attention with the advantages of high theoretical energy density, high abundance, and intrinsic safety stemming from their aqueous nature [6–10]. Despite its potential benefits, the use of Zn metal is hindered by associated challenges such as dendrite formation and unexpected side reactions at the anode/electrolyte interface, which may reduce the Zn plating/stripping Coulombic efficiency (CE) and cycle life [11–14].

To tackle these issues, extensive efforts have been dedicated to constructing artificial solid electrolyte interphase (SEI) that enables Zn^{2+} transportation while preventing water penetration to the Zn surface [15–17]. However, these interphases would lose the protective function due to the appearance of cracks or degradation during repeat volume changes of cycles, unlike *in situ* formed SEI which is self-repairable [18–21]. Hence, there is a strong desire to generate SEI through *in situ* electrolyte decomposition on the Zn surface. Increasing salt concentration to form water-in-salt (WIS) electrolytes is regarded as an effective strategy to facilitate SEI formation. Wang's group suggested that a fluorinated inorganic-organic composite SEI is formed through the decomposition of OTf^- in 21 m (mol/kg) LiTFSI + 7 m LiOTf electrolyte, which effectively safeguards the anode and prevents further electrolyte decomposition [22]. In addition, the use of 1 m $ZnTFSI_2$ + 20 m LiTFSI WIS electrolyte leads to the formation of the nanoparticle (NP)-shaped SEI, enabling the Zn plating/stripping CE up to 99.9% [23]. *In situ* insights into the interfacial evolution are crucial for further improvements in ZMBs. Previous work by our group focused on the direct tracking of the interfacial evolution on Cu metal surface to reveal the structure-performance correlations [24]. Two key fundamental issues still need consideration: First, the zincophilic Cu metal exhibits ultralow Zn nucleation barriers and further influences the deposition processes, which is partly different from practical interfacial evolution in ZMBs; Second, the interfacial reactions associated with Zn metal anode, such as shape change originated from the dissolution of Zn substrate, cannot be tracked on Cu metal surface, which has great impacts to the electrochemical performance in ZMBs. Therefore, the exploration of the interfacial evolution on the Zn metal anode is required to obtain a more comprehensive and predictive understanding of practical ZMBs.

In the present work, the real-time electrochemical processes, including the Zn nucleation, dynamic Zn deposition/dissolution, and SEI evolution on the Zn anode, are directly observed by *in situ* AFM in ZMBs with salt-in-water (SIW) and WIS electrolytes,

* Corresponding author.
E-mail address: ruiwen@iccas.ac.cn (R. Wen).

https://doi.org/10.1016/j.cclet.2024.109815
1001-8417/

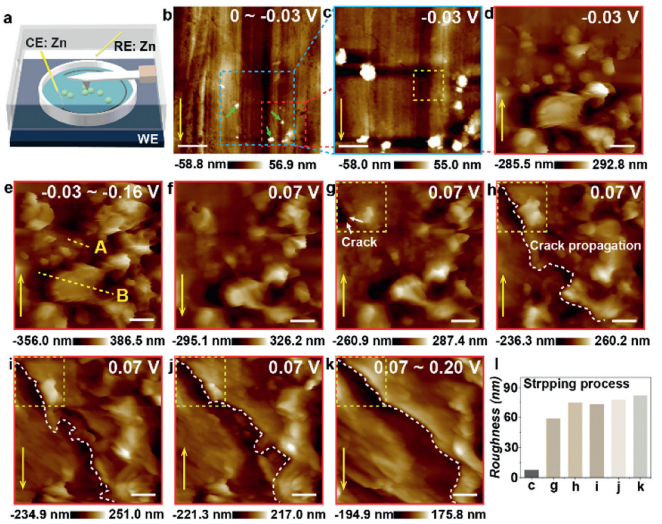

Fig. 1. *In situ* AFM monitoring of the Zn deposition/dissolution processes in SIW electrolyte. (a) Schematic illustration of the *in situ* electrochemical AFM cell. *In situ* AFM images of the Zn surface at different potentials of cathodic (b) 0 ~ −0.03 V, (c, d) −0.03 V and (e) −0.03 ~ −0.16 V, anodic (f-j) 0.07 V and (k) 0.07 ~ 0.20 V. l Quantitative analysis of the roughness in yellow dotted boxes of (c, g-k). The yellow arrows indicate the scanning direction. The scale bars are 2 μm in (b), 1 μm in (c), and 500 nm in (d-k).

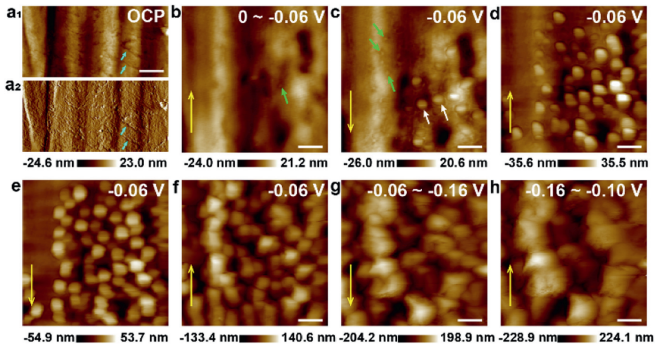

Fig. 2. *In situ* AFM images of the Zn anode surface at different potentials of (a_1) OCP, cathodic (b) 0 ~ −0.06 V, (c-f) −0.06 V, (g) −0.06 ~ −0.16 V, and (h) −0.16 ~ −0.10 V in WIS electrolyte. (a_2) Corresponding deflection image in (a_1). The yellow arrows indicate the scanning direction. The scale bars are 500 nm.

respectively. The homogeneous deposition and irreversible dissolution of the Zn, along with significant Zn substrate dissolution, clarify the degradation mechanism in SIW electrolyte. However, an anion-derived SEI film with a "plum-pudding" model is successfully captured on Zn anode, regulating the uniform deposition and dissolution in WIS electrolyte. In addition, the remaining folded nanostructure of the flexible SEI is beneficial for the protection of the electrode. These results provide direct insights into fundamental understanding of the correlations between surface morphological evolution and electrolytes during cycling, benefiting the optimization of battery design.

In situ AFM was performed to monitor the Zn plating/stripping processes on the Zn metal anode in SIW (1 m $Zn(TFSI)_2$) electrolyte. Fig. 1a provides the schematic illustration of the *in situ* electrochemical AFM cell, in which the Zn foil was used as the working electrode and Zn strips as the counter and reference electrodes. The cyclic voltammetry (CV) profile corresponding to the *in situ* AFM experiment is shown in Fig. S1 (Supporting information). Before conducting the *in situ* study, the Zn foil was carefully treated to remove the oxidation layer on its surface. The fresh Zn sample at open circuit potential (OCP) is presented in Fig. S2 (Supporting information). When charged from OCP to −0.03 V, some NPs appear on the electrode surface (as marked by the green arrows in Fig. 1b). The NPs gradually increase and accumulate (Fig. 1c), which can be ascribed to the initial stage of Zn deposition. Then, we zoomed in to investigate the interfacial processes in detail. As plating progresses, more Zn nuclei emerge randomly on the Zn anode surface and grow quickly (Figs. 1d and e). From the corresponding height section profiles (Fig. S3 in Supporting information), a notable difference in size between particles "A" and "B" can be observed. Such uneven size and spatial distribution of the initial Zn particles results in a heterogeneous electric field distribution on the Zn anode surface, which may result in the subsequent dendrite growth to pierce through the separator and cause an internal short circuit, ultimately leading to the death of the battery.

Figs. 1f-k show the dissolution process on the Zn surface. As the potential is shifted to 0.07 V, an evident dissolution occurs at the deposited products (Fig. 1f). Holding the potential at 0.07 V for 10 min, crack features appear on the Zn anode while the deposited Zn is not completely dissolved (Fig. 1g). Subsequently, the crack marked by white dotted lines becomes deeper and wider (Figs. 1h-k). Apparent shape change originating from the crack can also aggravate dendrite formation during the following cycle. In addition, due to the dissolution of the substrate, the roughness of the electrode surface in the yellow dotted boxes shows a gradual increase from 58.9 nm (Fig. 1g) to 81.7 nm (Fig. 1k) as the stripping progresses (Fig. 1l). The roughness of this region in Fig. 1c was only 7.5 nm. Such heterogeneous deposition and severe shape change of the Zn anode can lead to low CE and cycle life, ultimately accelerating the battery failure.

Applying WIS (1 m $Zn(TFSI)_2$ + 20 m LiTFSI) electrolyte was considered as an effective approach to stabilize the Zn anode by altering solvation structure, which can decrease water-induced side reactions and enhance Zn plating/stripping CE. Figs. S4 and S5 (Supporting information) show that the cells exhibit improved cycling stability, cycling life, and CE when using WIS electrolyte compared to SIW electrolyte, in accordance with reported work [23]. The CV curve obtained in WIS electrolyte is exhibited in Fig. S6 (Supporting information). *In situ* AFM was employed to monitor the charge and discharge processes to further explore the roles of the WIS electrolyte in interfacial regulation. At OCP, the original surface of the Zn anode exhibits a neatly arranged strip appearance with quite a few fine cracks (as indicated by blue arrows in Fig. 2a). Upon sweeping the potential from OCP to −0.06 V, the Zn anode becomes smooth and flat without evident cracks (Fig. 2b and Fig. S7 in Supporting information), which may be related to the formation of the amorphous products. Meanwhile, some protrusions marked by green arrows form on the Zn surface, which could be ascribed to the initial stage of Zn nucleation. Subsequently, the Zn nuclei increase and evolve into columnar sediments as plating continues (as marked by white arrows in Fig. 2c). Note that the deposits at the bottom of Fig. 2c are larger than those at the top because the scanning direction is from top to bottom, rather than the uneven deposition. Interestingly, the deposited Zn uniformly increases during the whole plating process (Figs. 2d-h), exhibiting a dendrite-free growth, which is greatly different from the deposition process in SIW electrolyte. *Ex situ* AFM characterization also confirms the uniform Zn deposition on the Zn surface (Fig. S8 in Supporting information). Furthermore, the increase in roughness variation is measured as 41.5 nm in WIS system from OCP to −0.16 V, significantly lower than the value of 84.3 nm observed in SIW system under the same condition (Fig. S9 in Supporting information), further indicating the uniform morphology. Fig. S10 (Supporting information) provides the corresponding three-dimensional (3D) AFM images, which clearly presents the topographical evolution.

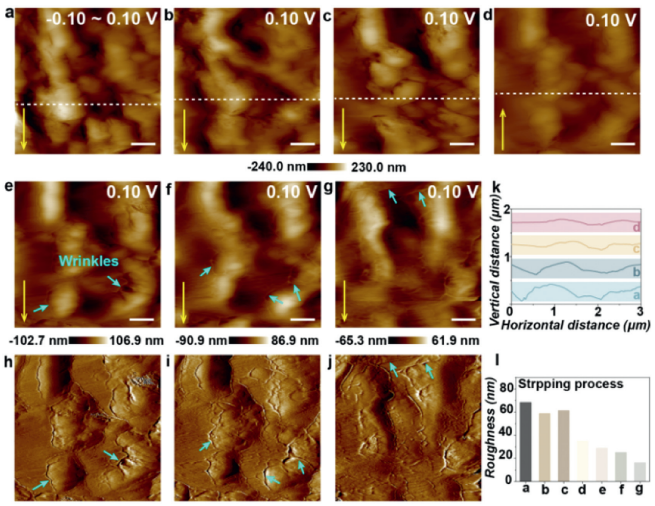

Fig. 3. *In situ* AFM images of the Zn anode surface at different potentials of (a) −0.10 ~ 0.10 V, (b-g) anodic 0.10 V in WIS system. (h-j) Corresponding deflection images in (e-g). (k) The profiles of Zn surface along the white dashed lines in (a-d). (l) Quantitative analysis of the roughness during the stripping process. The scale bars are 500 nm. The yellow arrows indicate the scanning direction.

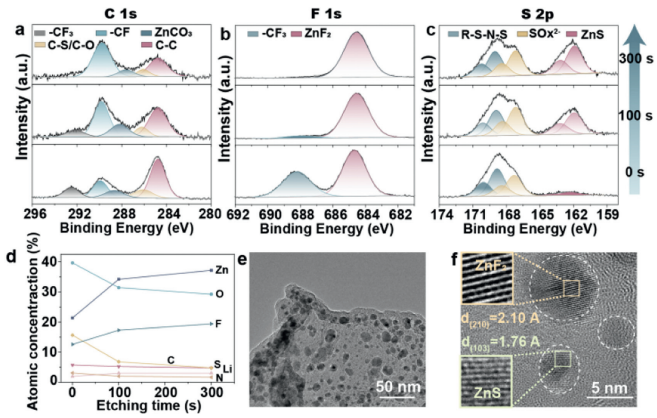

Fig. 4. XPS spectra of (a) C 1s, (b) F 1s, and (c) S 2p for Zn metal anode in WIS after Ar^+ sputtering for 0, 100, and 300 s. (d) Composition of electrode surface after various durations of Ar^+ sputtering on the Zn metal anode cycled in WIS system. (e, f) TEM images of the cycled Zn anode surface in WIS system.

Figs. 3a-g exhibit the Zn dissolution process in WIS electrolyte. When the potential positively shifted from −0.1 V to 0.1 V (Fig. 3a), the noticeable shrink occurs at the deposited Zn compared to the Zn in Fig. 2h, which corresponds to the conversion of Zn to Zn^{2+}. From the corresponding line profiles in Fig. 3k, the height difference changes from 275.7 ± 20.3 nm (Fig. 3a) to 114.0 ± 15.6 nm (Fig. 3d) along the vertical direction, revealing a uniform and fast dissolution process in WIS system. After a while, the deposited Zn dissolves to form a wrinkled structure (as indicated by the blue arrows) on the Zn anode surface; the number and length of wrinkles gradually increase as the dissolution process progresses (Figs. 3e-g). Ultimately, the average height of the wrinkles is approximately 7.6 ± 2.1 nm, and the mean width is around 47.1 ± 12.3 nm (Fig. 3g). Detailed ravines and valleys of wrinkles can be observed in corresponding deflection images (Figs. 3h-j). There are no evident cracks or pits on the Zn anode surface during the whole stripping process, showing the stability of Zn metal in WIS electrolyte. In addition, the roughness of the Zn anode surface exhibits a significant decrease from 68.6 nm in Fig. 3a to 16.5 nm in Fig. 3g, further indicating the excellent reversibility in the WIS system (Fig. 3l).

The deposited behaviors were also investigated by SEM in different electrolytes (Fig. S11 in Supporting information). In SIW electrolyte, the deposited Zn exhibits dendrite morphology at the current densities of 0.2 mA/cm^2 and 0.5 mA/cm^2. Interestingly, dense Zn deposition is observed in WIS electrolyte at a current density of 0.2 mA/cm^2. Increasing the current density to 0.5 mA/cm^2, there are thin flakes around the edges of the Zn block. It can be seen that the dendrite-free deposition can be achieved in WIS electrolyte at various current densities.

X-ray photoelectron spectroscopy (XPS) and transmission electron microscope (TEM) were employed to further disclose the chemical composition of the Zn anode surface. To avoid the abundant Zn deposition, the samples were obtained after the cell charging from OCP to −0.04 V instead of −0.06 V. The full XPS spectra are exhibited in Fig. S12 (Supporting information). In the C 1s spectra from XPS (Fig. 4a), except for the CF_3 component arising from the residual salt, we also observe the presence of CF, $ZnCO_3$, and C-O/C-S species on the cycled Zn anode, indicating the decomposition of electrolyte [25,26]. For the F 1s spectra, inorganic ZnF_2 is identified at approximately 684.6 eV, and the ratio of inorganic fluorine to organic fluorine increased with etching by Ar^+ (Figs. 4b and d) [27]. The percentage increases from 60.1% at the surface to 93.5% at 100 s and then about 100% at 300 s, indicating that inorganic fluoride enriches in the inner layer. In addition to ZnF_2, inorganic ZnS (~162.0 eV) is observed in S 2p spectra on the Zn anode due to the decomposition of WIS electrolyte, which also increases with Ar^+ sputtering (Fig. 4c). This trend is commonly referred to as the "bilayer SEI" in the literature [28,29], with the inner layer containing mainly inorganic species and the outer layer predominantly composed of organic species.

In addition, TEM was employed to further analyze the Zn anode surface to confirm the presence of interphase. It shows a "plum-pudding" model, in which crystal particles are embedded in the amorphous film (Fig. 4e and Fig. S13 in Supporting information) [30]. From the high-resolution TEM in Fig. 4f, it is observed that the small crystalline domains dispersed randomly throughout the amorphous film are mainly ZnF_2 and ZnS, which is consistent with XPS analysis. The amorphous matrix is likely the organic/polymeric species originating from $TFSI^-$. The DFT calculations have shown that the reduction potential of $TFSI^-$ would be increased due to its interaction with Zn^{2+}, inducing the formation of SEI [31]. Therefore, the wrinkle structure observed *in situ* AFM experiments is a ZnF_2-rich SEI layer, which is considered as an electron barrier that inhibits the reduction of water while facilitating the migration of Zn^{2+} [32,33].

In contrast, the Zn dendrite was observed in SIW electrolyte at the same condition (Fig. S14 in Supporting information). In addition, the O 1s spectra in SIW electrolyte show an obvious ZnO signal (Fig. S15 in Supporting information). This can be attributed to the solvation of Zn^{2+} by dipolar water molecules in dilute solutions. As a result, the O-H bonds are considerably weakened and undergo deprotonation, leading to the transformation into electrochemically inactive ZnO, thereby passivating the metal surface and inducing uneven Zn deposition [34].

Based on the *in situ* observations and *ex situ* characterizations, the interfacial reaction mechanisms of the Zn anode with different electrolytes upon cycling are proposed. Figs. 5a-d depict the dynamic evolution in SIW electrolyte. Zn^{2+} remains adequately hydrated in its primary solvation sheath because sufficient free water is available in SIW electrolyte (Fig. 5a), which induces the formation of inactive ZnO. As the potential is negatively shifted, the Zn nuclei unevenly appear on the Zn anode, which increases the heterogeneous distribution of the electric field (Fig. 5b). During the subsequent plating process, Zn tends to deposit at the tip of Zn nuclei because of the "tip effect", resulting in the vertical growth of Zn and then forming dendrite morphology (Fig. 5c). Such uneven

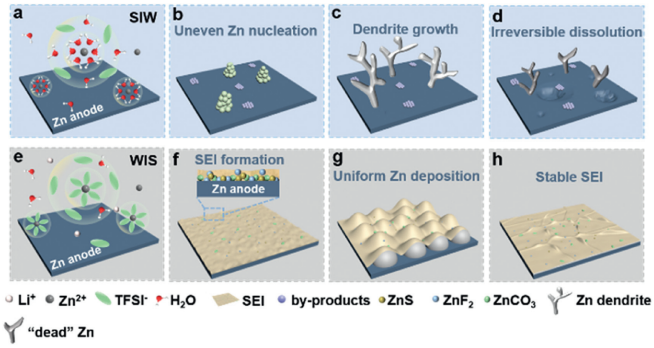

Fig. 5. Schematic illustration of the structural evolution and reaction mechanisms. Interphase formation and Zn deposition/dissolution processes on the Zn anode surface in (a-d) SIW and (e-h) WIS electrolytes, respectively.

Zn deposition may be linked to the formation of electrochemically inactive ZnO. During the stripping process, the deposited Zn cannot be decomposed completely. Moreover, the dissolution of the Zn substrate causes visible cracks or pits on the anode surface, exacerbating the non-uniformity and altering its shape (Fig. 5d). Such interfacial processes of uneven deposition and irreversible dissolution ultimately lead to the penetration of Zn dendrite during the long-life cycles, which may cause the safe risks.

In WIS electrolyte, the Zn^{2+} cations are solvated by $TFSI^-$ when sufficient salt anions are present, which leads to the decomposition of $TFSI^-$ and then form SEI on the Zn anode (Fig. 5e). The on-site formed SEI exhibits a "plum-pudding" model, with NPs composed of ZnF_2, $ZnCO_3$ and ZnS (plum) embedded in the organic film (pudding) decomposed by electrolyte (Fig. 5f). The upper layer of SEI is mainly organic components, while the inner layer is predominantly inorganic. Such SEI possesses a high ion conductivity and evenly covers the Zn anode surface. Furthermore, the high ZnF_2/Zn interface energy can induce uniform Zn nucleation and dendrite-free growth (Fig. 5g). During the stripping process, the deposited Zn is almost completely dissolved, and there is no evident dissolution on the Zn substrate under the protection of the SEI layer, showing excellent deposition/dissolution reversibility in WIS system. Meanwhile, the SEI evolves into the wrinkle structure due to the release of in-plane compressive stress (Fig. 5h). The on-site generated SEI has sufficient flexibility to withstand deformation during cycling, which ensures that the breaking and formation of the SEI consumes fewer active materials. These results visually provide the functions of the SEI layer on Zn deposition/dissolution, offering support for the optimization and design of high-quality SEI for stable Zn metal anodes.

In conclusion, *in situ* AFM was applied to disclose the interfacial evolution and dynamic mechanisms on the Zn metal anode in a working battery. By altering the solvation shell, a uniform SEI film forms on the Zn metal anode to inhibit water-induced parasitic reactions and further electrolyte decomposition in WIS system. The morphology, structure, and chemical properties of the SEI film are deeply analyzed. Furthermore, the SEI can effectively regulate the nucleation and growth behaviors of Zn during the plating process. Dendrite-free plating and reversible plating/stripping processes contribute to the stabilization of the interface. Our work provides a useful way to detect and manipulate the interfacial evolution of the Zn anode at nanoscale, which promotes a fundamental understanding of the intrinsic characteristics of SEI and further guides the interface optimization.

Declaration of competing interest

The authors declare that they have no known competing financial interests or personal relationships that could have appeared to influence the work reported in this paper.

Acknowledgments

This work was financially supported by the National Key R&D Program of China (No. 2021YFB2500300), the CAS Project for Young Scientists in Basic Research (No. YSBR-058), the National Science Foundation of China (No. 22205241) and the National Postdoctoral Program for Innovative Talents (No. BX20220306) of the Chinese Postdoctoral Science Foundation.

Supplementary materials

Supplementary material associated with this article can be found, in the online version, at doi:10.1016/j.cclet.2024.109815.

References

[1] C.S. Lai, Y. Jia, L.L. Lai, et al., Renew. Sustain. Energy Rev. 78 (2017) 439–451.
[2] J. Zheng, M.S. Kim, Z. Tu, et al., Chem. Soc. Rev. 49 (2020) 2701–2750.
[3] H. Kim, J. Hong, K.Y. Park, et al., Chem. Soc. Rev. 49 (2020) 2701–2750.
[4] A. Yoshino, Angew. Chem. Int. Ed. 51 (2012) 5798–5800.
[5] L. Chen, C. Chen, L. Jin, et al., Energy Environ. Sci. 14 (2021) 955–964.
[6] Z. Tie, Y. Zhang, J. Zhu, S. Bi, Z. Niu, J. Am. Chem. Soc. 144 (2022) 10301–10308.
[7] J. Zheng, D.C. Bock, T. Tang, et al., Nat. Energy 6 (2021) 398–406.
[8] C. Li, R. Kingsbury, A.S. Thind, A. Shyamsunder, et al., Nat. Commun. 14 (2023) 3067.
[9] Y. Wang, J. Yin, J. Zhu, Chin. J. Chem. 40 (2022) 973–988.
[10] M. Zhang, H. Peng, K. Sun, et al., Chin. J. Chem. 40 (2022) 2763–2772.
[11] X. Zheng, Z. Liu, J. Sun, et al., Nat. Commun. 14 (2023) 76.
[12] Q. Yang, Q. Li, Z. Liu, et al., Adv. Mater. 32 (2020) 2001854.
[13] T. Huang, K. Xu, N. Jia, et al., Adv. Mater. 35 (2023) 2205206.
[14] S. Cai, G. Chang, J. Hu, et al., Chin. J. Chem. 41 (2023) 1697–1704.
[15] Z. Yi, G. Chen, F. Hou, L. Wang, J. Liang, Adv. Energy Mater. 11 (2021) 2003065.
[16] L. Kang, M. Cui, F. Jiang, et al., Adv. Energy Mater. 8 (2018) 1801090.
[17] X. Wu, Y. Dai, N.W. Li, X.C. Chen, L. Yu, eScience (2023) 100173.
[18] W. Zhang, G. He, Angew. Chem. Int. Ed. 62 (2023) e202218466.
[19] X. Zeng, J. Mao, J. Hao, et al., Adv. Mater. 33 (2021) 2007416.
[20] P. Xiong, Y. Kang, N. Yao, et al., ACS Energy Lett. 8 (2023) 1613–1625.
[21] S. Jin, F. Duan, X. Wu, et al., Small 18 (2022) 2205462.
[22] L. Suo, O. Borodin, W. Sun, et al., Angew. Chem. Int. Ed. 55 (2016) 7136–7141.
[23] J. Wang, J.X. Tian, G.X. Liu, Z.Z. Shen, R. Wen, Small Methods 7 (2023) 2300392.
[24] E. Hu, X.Q. Yang, Nat. Mater. 17 (2018) 480–481.
[25] K. Gao, S. Li, J. Liu, et al., Adv. Funct. Mater. 33 (2023) 2307641.
[26] L. Cao, D. Li, T. Pollard, et al., Nat. Nanotechnol. 16 (2021) 902–910.
[27] W. Wang, S. Chen, X. Liao, et al., Nat. Commun. 14 (2023) 5443.
[28] S. Di, X. Nie, G. Ma, et al., Energy Stor. Mater. 43 (2021) 375–382.
[29] D. Li, L. Cao, T. Deng, S. Liu, C. Wang, Angew. Chem. Int. Ed. 60 (2021) 13035–13041.
[30] H. Wu, H. Jia, C. Wang, J.G. Zhang, W. Xu, Adv. Energy Mater. 11 (2021) 2003092.
[31] H. Qiu, X. Du, J. Zhao, et al., Nat. Commun. 10 (2019) 5374.
[32] Y. Chu, S. Zhang, S. Wu, et al., Energy Environ. Sci. 14 (2021) 3609–3620.
[33] Y. An, Y. Tian, K. Zhang, et al., Adv. Funct. Mater. 31 (2021) 2101886.
[34] W. Hu, J. Ju, N. Deng, et al., J. Mater. Chem. A 9 (2021) 25750–25772.